

Article

# Geomechanical Studies on Granite Intrusions in Alxa Area for High-Level Radioactive Waste Disposal

Cheng Cheng \*, Xiao Li, Shouding Li and Bo Zheng

Key Laboratory of Shale Gas and Geoenvironment, Institute of Geology and Geophysics, Chinese Academy of Sciences, Beijing 100029, China; lixiao@mail.iggcas.ac.cn (X.L.); lsdlyh@mail.iggcas.ac.cn (S.L.); zhengbo@mail.iggcas.ac.cn (B.Z.)

\* Correspondence: cheng@mail.iggcas.ac.cn; Tel.: +86-10-8299-8405

Academic Editor: Vincenzo Torretta

Received: 14 July 2016; Accepted: 12 December 2016; Published: 16 December 2016

**Abstract:** Geological storage is an important concept for high-level radioactive waste (HLW) disposal, and detailed studies are required to protect the environment from contamination by radionuclides. This paper presents a series of geomechanical studies on the site selection for HLW disposal in the Alxa area of China. Surface investigation in the field and RQD analyses on the drill cores are carried out to evaluate the rock mass quality. Laboratory uniaxial and triaxial compressive tests on the samples prepared from the drill cores are conducted to estimate the strength properties of the host rock. It is found that the NRG sub-area has massive granite intrusions, and NRG01 cored granite samples show the best rock quality and higher peak strength under various confinements (0–30 MPa). NRG01 granite samples are applied for more detailed laboratory studies considering the effects of strain rate and temperature. It is observed that the increasing strain rate from  $1.0 \times 10^{-5}$ – $0.6 \times 10^{-2} \cdot s^{-1}$  can lead to a limited increase on peak strength, but a much more violent failure under uniaxial compressive tests on the NRG01 granite samples, and the temperature increasing from 20 °C–200 °C may result in a slight increase of UCS, as well as more ductile post-peak behavior in the triaxial compressive tests.

**Keywords:** high-level radioactive waste disposal; geomechanical study; site selection; rock quality; rock strength; strain rate; temperature

## 1. Introduction

Deep geological disposal has been widely accepted as a promising method for the isolation of high-level radioactive waste (HLW) from our environment by the international nuclear community. It is required to carry out extensive research, including tectonic movement, hydraulic conductivity, climate change, engineering stability, human activities, etc., to ensure that the biosphere can be protected from the pollution of radionuclides for a long period. The geomechanical study is of great importance to evaluate the structural characteristics, short-term and long-term deformation and damage behavior of host rock mass, and it has played significant roles in site selection and field experiments in the underground research laboratories (URLs) in many countries [1–9].

In China, the plan for HLW disposal includes three steps: (1) laboratory studies and site selection for a repository (2006–2020); (2) underground in situ tests (2021–2040); and (3) repository construction (2041–2050) followed by operation [10]. In the past few years, site characterization and selection focused on Beishan area, Gansu Province in northwestern China, and a series of studies has been conducted involving geological mapping, surface and borehole geophysical survey, hydraulic conductivity testing, in situ stress measurement, rock mechanical testing, and so on [4,11,12]. For a comparative study during the site selection period, Alxa area in Inner Mongolia Autonomous Region is chosen to be

a new candidate area due to the occurrence of large blocks of granite intrusions (Figure 1), which is similar to Beishan area.

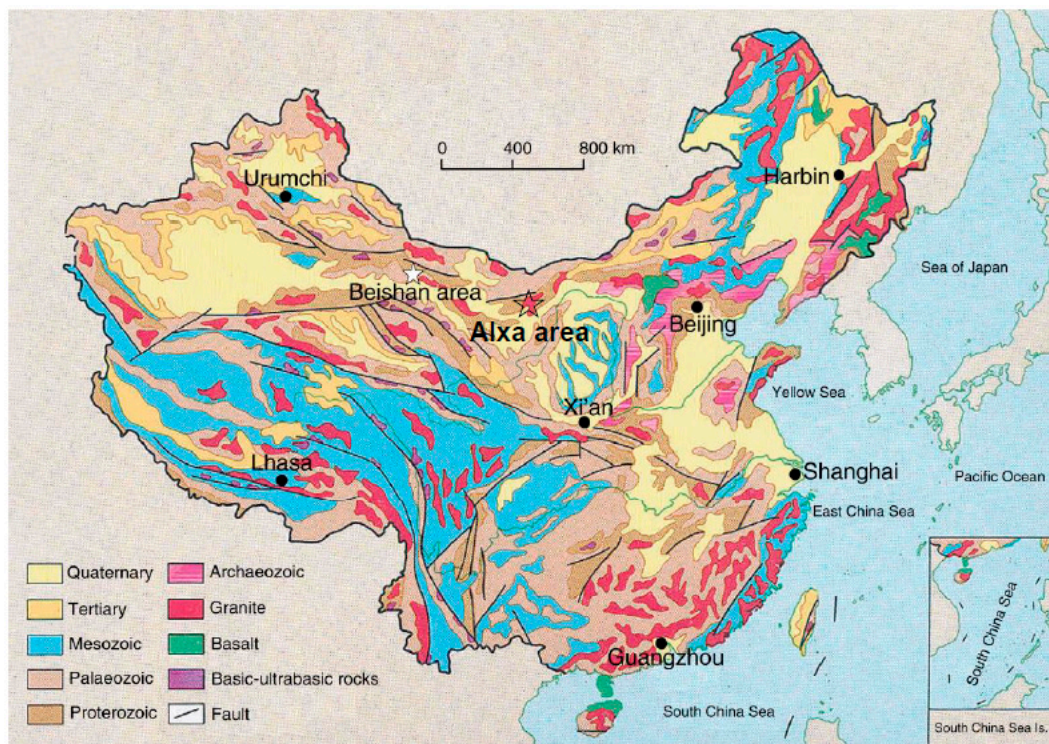


**Figure 1.** Geographical location of Alxa area in Inner Mongolia Autonomous Region, China. Modified after [4].

Various investigations and research have been carried out in Alxa area. Geographical studies show that Alxa area is located in the Gobi Desert in North China and has a relatively flat landscape with some small hills. The annual amount of evaporation is as high as 30-times the rainfall in this area; hence, it is an extremely arid region with very few people living there [13]. According to the tectonic analyses, this area is situated in the region between the central part of the southern Central Asian Orogenic Belt (CAOB) and the Alxa Block [14,15]. Velocity field of crustal movement based on GPS shows that the crust is relatively stable in Alxa area (Figure 2) [16]. Based on the general geological features of Alxa area described above, the Tamusu (TMS) and Nuorigong (NRG) regions are selected as two sub-areas; they are both located in the stable zones between the faults, and two sub-vertical boreholes in each of the two sub-areas were drilled (TMS01, TMS02, NRG01 and NRG02) (Figure 3). Geophysical and hydrological studies have also been conducted in these two sub-areas, and some related results have been reported in [13,17].

However, the geomechanical properties on the granite intrusions in Alxa area have not been studied so far. In this work, rock mass structure surveys on the exposures in the two sub-areas and statistical analyses on the RQD (rock quality designation index) values obtained from the drill core logs were carried out (Section 2). Mineral compositions of the cores are studied, and the strength properties of the cored samples are analyzed based on laboratory testing results, as well as the mineral distributions (Section 3). Excavation-induced disturbance and earthquakes may lead to different magnitudes of dynamic loading; therefore, mechanical properties on cored samples are studied under different axial strain rates (Section 4). As the fission of HLW can produce heat, which may influence the stability of the surrounding rock, laboratory tests were conducted to study the thermal effect on the cored samples (Section 5). Based on these investigations and analyses, an engineering geological assessment on site selection for HLW disposal in Alxa area is discussed in Section 6.

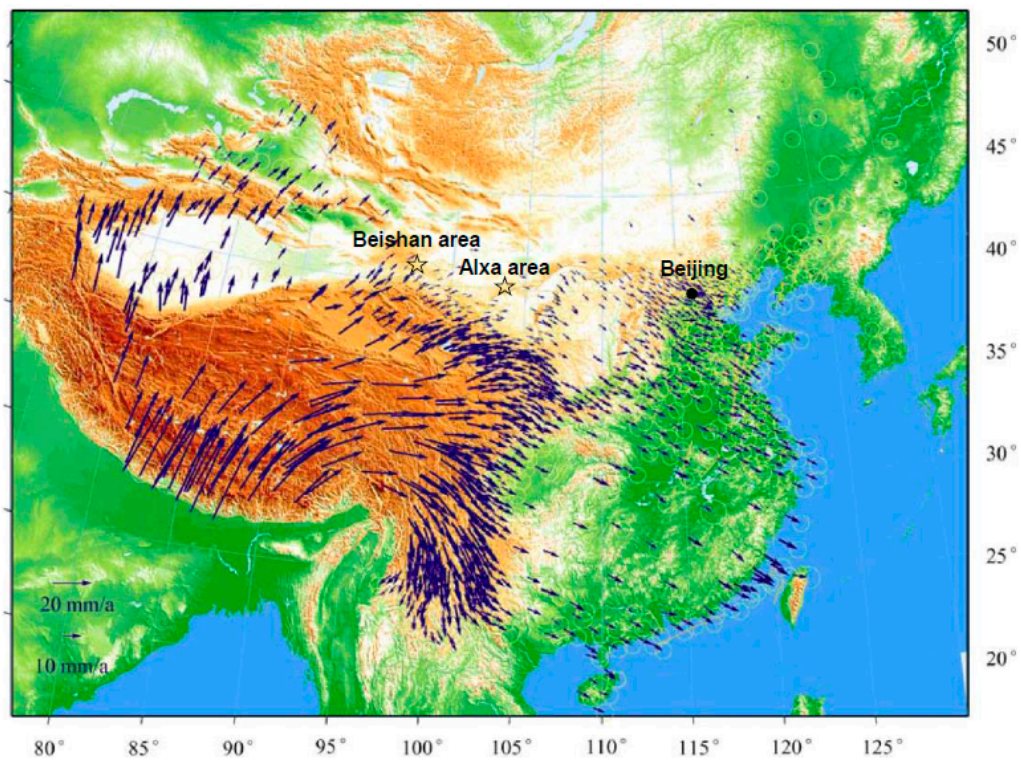


**Figure 2.** Velocity field of crustal movement in the Chinese mainland relative to the stable Eurasia based on GPS. Modified from [16].

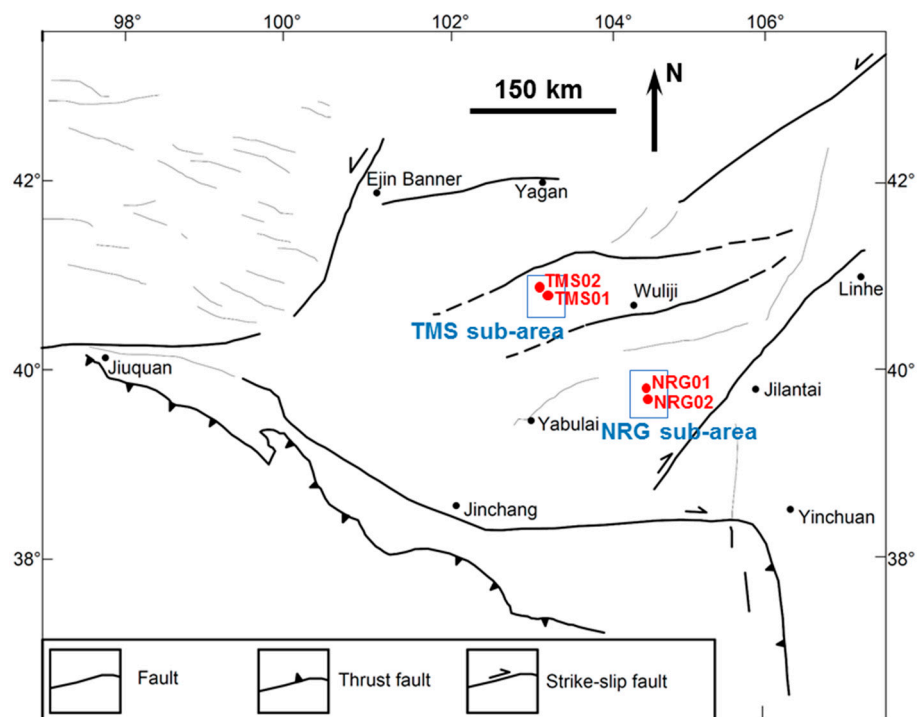


**Figure 3.** Schematic map of main geological structures in Alxa area. Modified after [15].

## 2. Rock Mass Structure and Characterization

### 2.1. Rock Mass Structure Studied from Surface Exposures

A surface investigation has been carried out in both the TMS and NRG sub-areas. In the TMS sub-area, borehole TMS01 is surrounded by many small denudation hills, and many outcrops can be found. The grey and dark rock mass is quite weathered with a large number of joints (Figure 4a). The regions around borehole TMS02 is almost flat and covered by Quaternary sands (Figure 4b); however, some outcrops are found about 2500 m away from this borehole (Figure 4c). The jointed granitic rock mass has the same pink color as the cored samples extracted from borehole TMS02.

The scanning line method has been applied to survey the rock mass structures. One thousand two hundred twenty eight and 1713 discontinuities have been investigated in these two regions drilled by boreholes TMS01 and TMS02, respectively. It is observed that the discontinuities are mainly shear joints. Figure 5 presents the distribution of dips and strikes of discontinuities measured in the region around borehole TMS01. It is apparent that most of the discontinuities have high dip angles ranging from  $50^{\circ}$ – $85^{\circ}$ . The strike covers almost all directions, and the optimal strike falls into the range of  $060$ – $080$  degrees. According to the corresponding survey in the outcrops drilled by borehole TMS02 shown in Figure 6, most of the discontinuities also have high dip angles ( $55^{\circ}$ – $80^{\circ}$ ), while the range of  $15^{\circ}$ – $30^{\circ}$  is a secondary most distributed dip angle. Two optimal strike ranges are  $150$ – $130$  degrees and  $030$ – $060$  degrees.

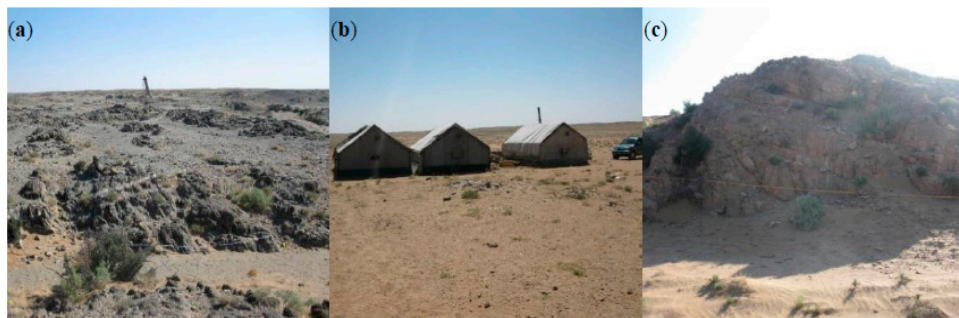


**Figure 4.** Typical topography of TMS sub-area, including two regions around (a) borehole TMS01 and (b) borehole TMS02; (c) an outcrop  $S60^{\circ}E$  of Borehole TMS02 with a distance of about 2500 m between them.

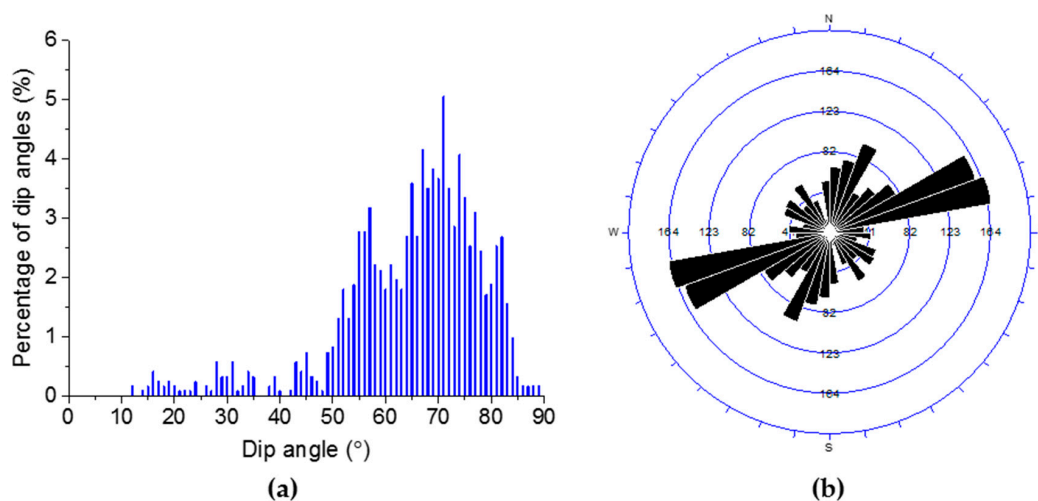


**Figure 5.** Rock structure survey from natural outcrops around borehole TMS01. (a) Percentage of dip angles; and (b) rosette plot of the strike of the measured discontinuities.

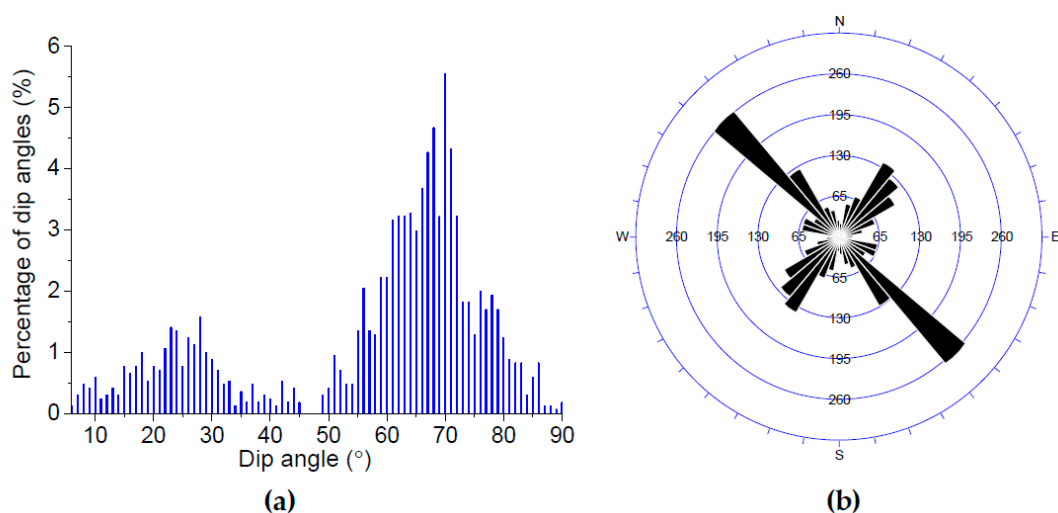


**Figure 6.** Rock structure survey from natural outcrops S60°E of borehole TMS02 with a distance of about 2500 m between them. (a) Percentage of dip angles; and (b) rosette plot of the strike of the measured discontinuities.

The NRG sub-area is mainly covered by Quaternary sands, and very few natural rock exposures can be observed (Figure 7a). Fortunately, there are many quarries that expose massive granite. However, very few discontinuities can be observed (Figure 7b), and a large number of intact granite blocks explored in the quarries show that the rock quality is very good (Figure 7c).

Comparatively, based on the surface investigation in the two sub-areas, the TMS sub-area has suffered from much more geological disturbances, and the outcrops show that the near-surface rock mass is quite jointed and discontinuous; whereas the near-surface rock mass in the NRG sub-area is very massive, and very few discontinuities can be observed.

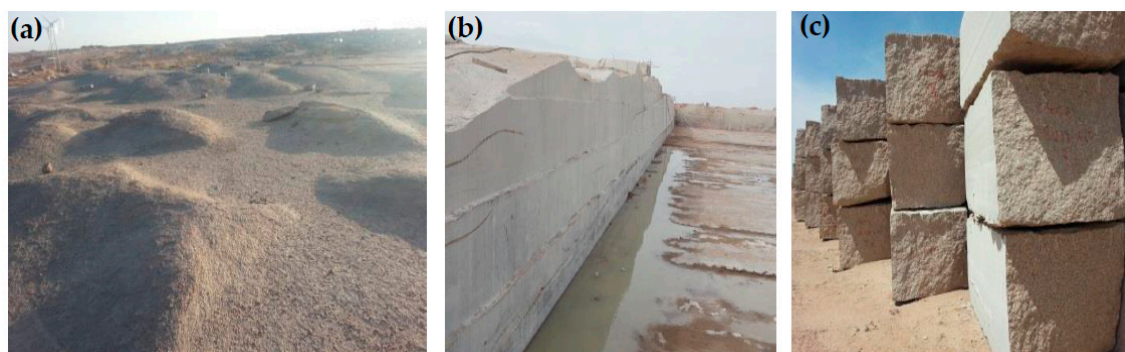


**Figure 7.** (a) Typical topography of the NRG sub-area; (b) an open pit; and (c) large intact granite blocks in a quarry of this sub-area.

## 2.2. RQD Analyses from Drilling Cores

RQD developed by Deere [18] is a widely-used method to estimate the underground rock mass quality before excavation. It is defined as the intact core pieces longer than 100 mm in the total length of a core run. RQD closer to 100% means better quality of the rock mass, and an RQD-based classification is always adopted as follows: 0%~25% (very poor rock quality), 25%~50% (poor rock quality), 50%~75% (fair rock quality) and 90%~100% (very good rock quality) [4,18].

The distribution of RQD along with the depth measured based on the core logs from the four boreholes are presented in Figure 8. It should be noted that for boreholes TMS01, NRG01 and NRG02, RQD are measured carefully by each of the core runs, while for borehole TMS02, some average values

are used. However, this does not influence the comparative analyses on the rock mass quality among the four boreholes.

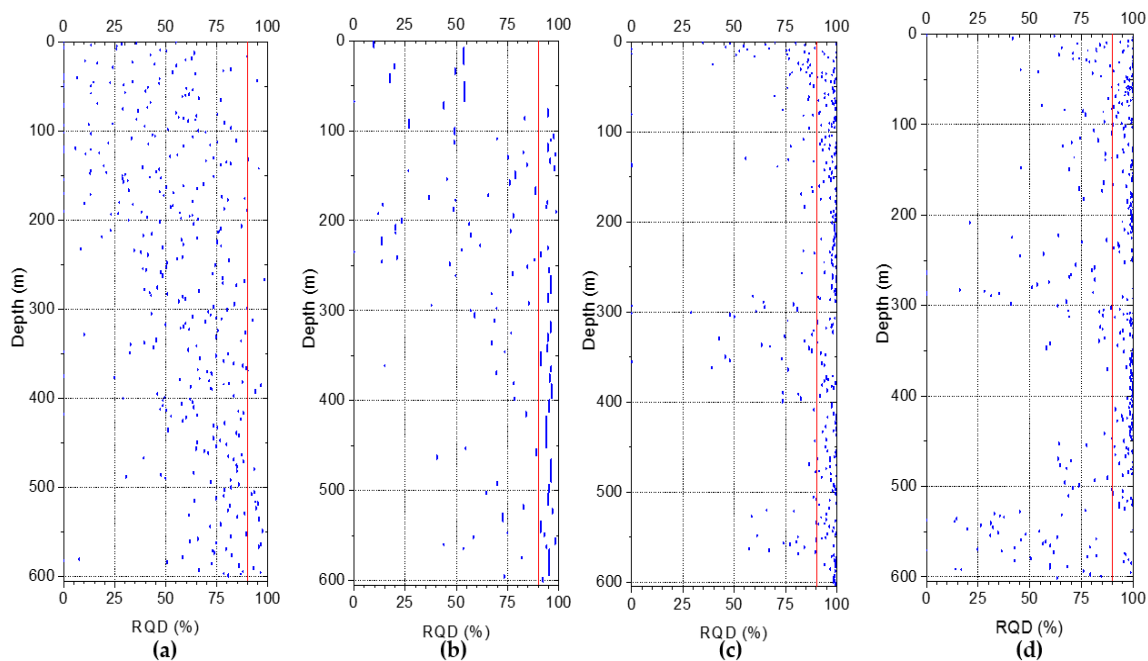


**Figure 8.** Scatter plots of RQD versus depth in the boreholes of: (a) TMS01; (b) TMS02; (c) NRG01; and (d) NRG02. The red lines indicate an RQD value of 90%.

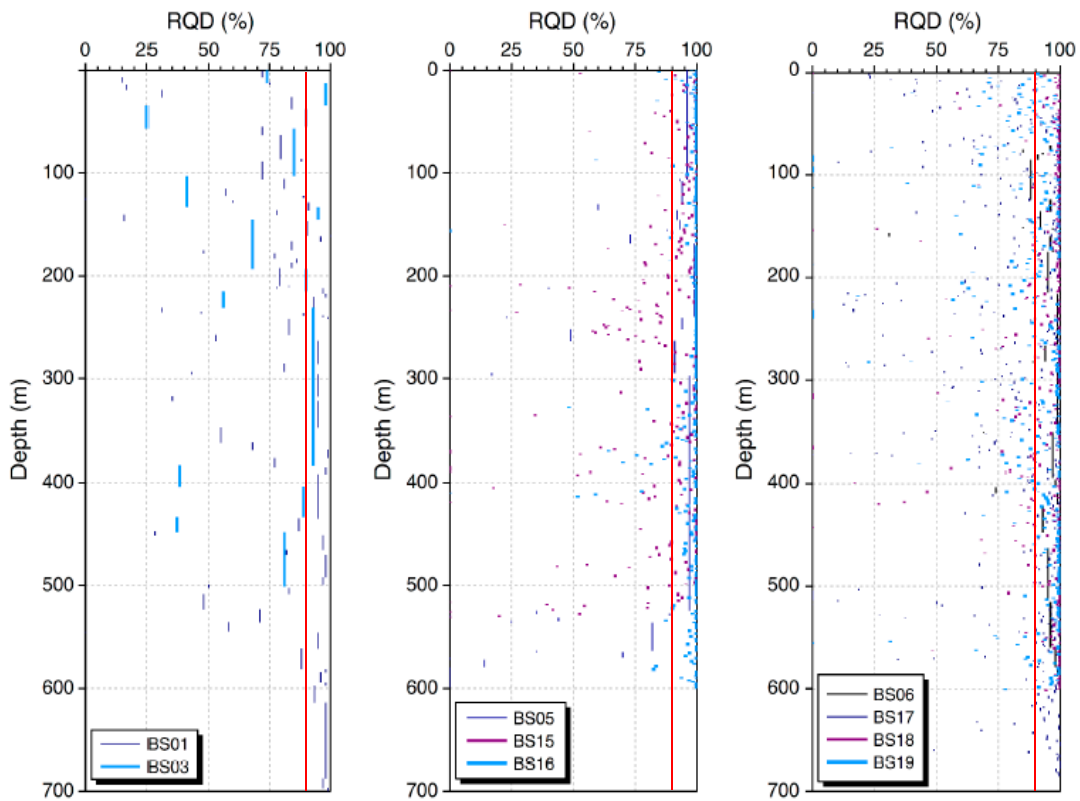
According to Figure 8, RQD measured for borehole NRG01 shows the best quality, and most of the RQD values are higher than 90%, although some poor cases are observed at the depths around 300 m and 540 m. For the boreholes TMS01 and TMS02, the rock quality is very poor in the shallower depth, and it becomes better with the increase of depth; however, it is still not good enough at the depth of 400~600 m. For borehole NRG02, rock mass quality in the shallower depth is better than the cases in TMS01 and TMS02, but it becomes very poor at the depth of 400~600 m.

Figure 9 shows the RQD measurements in the boreholes drilled in Beishan (BS) area [4], and it can be found that the boreholes BS05 and BS06 show the best rock mass qualities. In the Alxa area, only borehole NRG01 shows comparable RQD values with these two boreholes in the Beishan area.

A detailed comparison on the proportion of different rock mass qualities based on the boreholes of TMS01, TMS02, NRG01, NRG02, as well as the nine boreholes from Beishan area [4] is presented in Table 1 and Figure 10. It is obvious to see that the boreholes NRG01 and NRG02 show quite better rock mass quality than the boreholes TMS01 and TMS02, while the borehole NRG01 shows better quality than the average condition of the nine boreholes from the Beishan area.

**Table 1.** Proportion of different rock mass qualities based on the RQD analyses.

RQD (%)	TMS01	TMS02	NRG01	NRG02	Beishan [4]
0–25 (very poor)	16.62%	12.07%	2.08%	3.64%	2.90%
25–50 (poor)	21.41%	12.93%	2.08%	5.58%	3.80%
50–75 (fair)	32.68%	20.69%	6.93%	12.62%	7.30%
75–90 (good)	22.25%	17.24%	13.86%	13.83%	17.90%
90–100 (excellent)	7.04%	37.07%	75.06%	64.32%	68.10%



**Figure 9.** Scatter plots of RQD versus depth in the boreholes of the Beishan (BS) area in Gansu Province, China. The red lines indicate an RQD value of 90%. Modified from [4].

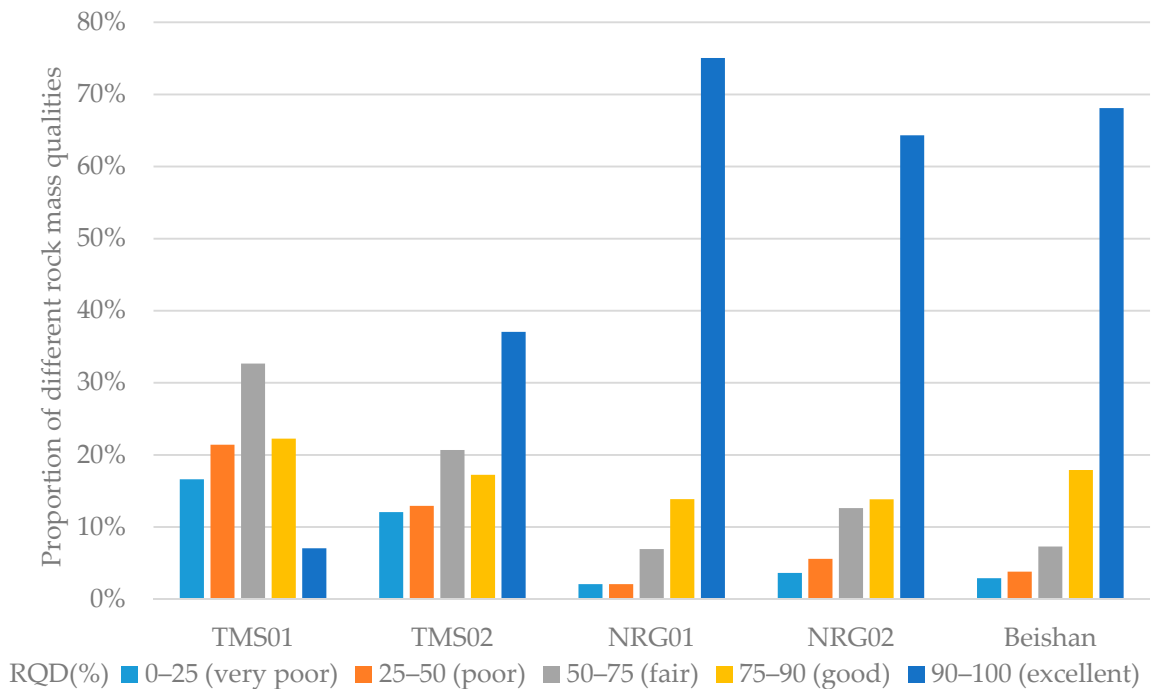


**Figure 10.** Proportion of different rock mass qualities based on the RQD analyses.

### 2.3. Discussion

According to both the investigation on surface exposures and RQD classifications in the two sub-areas, it can be seen that the rock in the NRG sub-area is more massive than that in the TMS

sub-area. Furthermore, RQD values show that the cores in borehole NRG01 have better rock mass quality, and RQD values in NRG01 are close to the best cases in Beishan area.

Consequently, more detailed research should be conducted in the region around borehole NRG01. In next section, some laboratory studies on the cored samples from NRG01 will be carried out. For comparison, corresponding experiments will also be performed on some samples from borehole TMS01.

### 3. Laboratory Studies on the Strength Properties of Cored Samples

Strength is a very important property for the stability of the surrounding rock. This section will study the strength properties of the intact granite samples from boreholes TMS01 and NRG01 under different confinements.

#### 3.1. Rock Samples

The samples are prepared from the drilling cores from boreholes TMS01 and NRG01 at the depth of 500~600 m. All of the samples are intact and have the same size of 100 mm in height and 50 mm in diameter. The preparation precision is based on the ISRM (International Society for Rock Mechanics) suggested method [19,20].

Figure 11 presents the pictures of the typical samples from boreholes TMS01 and NRG01. Figure 11c,d shows the cross-sections of the samples in Figure 11a,b. The grey granite sample from borehole TMS01 has about 45% plagioclase (grain size 2.0~4.0 mm), about 25%~30% quartz (grain size 1.5~3.5 mm), about 10% hornblende, about 10% K-feldspar, about 5% biotite and about 5% of other dark minerals. The pink granite sample from borehole NRG01 has about 35% K-feldspar (grain size 2.0~22.0 mm), about 35% plagioclase (grain size 2.0~5.0 mm), about 25% quartz (grain size 2.0~4.0 mm) and about 5% other dark minerals.

Apparently, NRG01 granite is more coarse and heterogeneous than TMS01 granite. Besides, TMS01 samples are observed to be foliated, to some extent, by the formation of some gneissosity, while NRG01 granite samples are more massive and unfoliated.

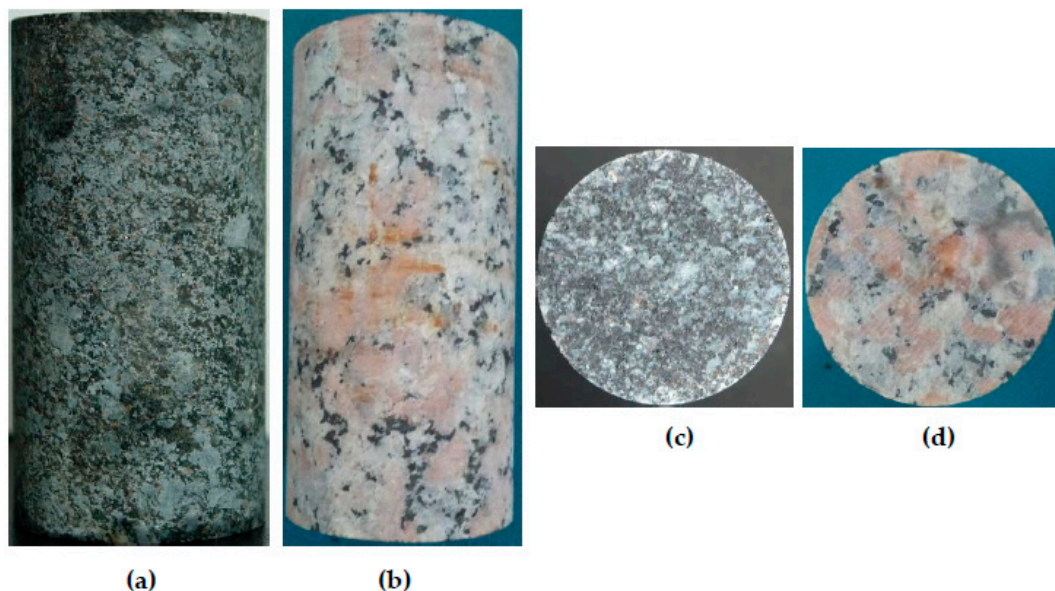


**Figure 11.** Typical samples (height: 100 mm; diameter: 50 mm) from the boreholes of TMS01 (a,c) and NRG01 (b,d).

### 3.2. Strength Properties of Cored Samples under Different Confinements

Uniaxial and conventional triaxial compressive tests on the samples from both boreholes TMS01 and NRG01 have been carried out in a servo-controlled stiff test machine with the axial strain rate of  $1.0 \times 10^{-5} \cdot \text{s}^{-1}$ . The peak strength of the samples under various confinements (0~30 MPa) is plotted in Figure 12a. For comparison, the test results on BS06 granite samples from the Beishan area in Gansu Province are also presented [21]. It is apparent that the strength values of NRG01 samples under various confinements are close to the values of BS06 samples, while they are significantly higher than the strength values of TMS01 samples.

Peak strength envelopes are plotted in Figure 12a according to the Hoek–Brown criterion [22] shown as:

$$\sigma'_1 = \sigma'_3 + \sigma_{ci} (m_b \sigma'_3 / \sigma_{ci} + s)^a \quad (1)$$

where  $\sigma'_1$  and  $\sigma'_3$  are the maximum and minimum effective principal stresses,  $\sigma_{ci}$  is the uniaxial compressive strength (UCS) of intact rock and  $m_b$  is a reduced value of the intact rock material parameter  $m_i$ , which is usually determined by a series of triaxial compressive tests under various confinements and is given by:

$$m_b = m_i \exp[(GSI - 100) / (28 - 14D)] \quad (2)$$

where *GSI* (Geological Strength Index) is developed by Hoek et al. [23] and can be used to estimate the strength reduction of rock mass considering the rock structure and joint surface conditions and *D* is a factor depending on the degree of disturbance, varying from zero for undisturbed rock to one for very disturbed rock masses.

*s* and *a* in Equation (1) are two constants for rock mass and are given by:

$$s = \exp[(GSI - 100) / (9 - 3D)] \quad (3)$$

$$a = \frac{1}{2} + \frac{1}{6} \left( e^{-\frac{GSI}{15}} - e^{-\frac{20}{3}} \right) \quad (4)$$

In the present study, we focus on the strength properties of the intact rock based on the tests on the cored samples; *GSI* = 100 and *D* = 0 are used, and so  $m_b = m_i$ , *s* = 1.0 and *a* = 0.5. Figure 12a gives the fitted peak strength envelopes for the intact rock samples from the boreholes of TMS01, NRG01 and BS06. In the future, more detailed knowledge on the rock structure and joint conditions can be considered to study the reduced strength properties with the Hoek–Brown criterion.

Another one of the most widely-used strength criteria in rock engineering application is the Coulomb–Mohr criterion, which is expressed as:

$$\tau = c + \sigma_n \tan \phi \quad (5)$$

where shear strength  $\tau$  is composed of a constant cohesion *c* and a frictional component dependent on normal stress  $\sigma_n$  and  $\phi$  is the inner frictional angle.  $\sigma_n$  and  $\tau$  are always calculated using the stress transformation Equations (6) and (7) [24] given by:

$$\sigma_n = \frac{1}{2}(\sigma_1 + \sigma_3) + \frac{1}{2}(\sigma_1 - \sigma_3) \cos 2\beta \quad (6)$$

$$\tau = \frac{1}{2}(\sigma_1 - \sigma_3) \sin 2\beta \quad (7)$$

where  $\beta$  is the acute angle between the shear plane and the direction of  $\sigma_3$ , and it has a relationship with  $\phi$  shown as:

$$\beta = \frac{\pi}{4} + \frac{\phi}{2} \quad (8)$$

Consequently, the shear strength  $\tau$  and normal stress  $\sigma_n$  can be obtained based on the peak strength values under different confinements, and they are plotted in Figure 12b. Linearly-fitted Coulomb–Mohr envelopes are also presented.

Based on the peak strength of different granite samples under different confinements and the calculated Hoek–Brown and Coulomb–Mohr parameters presented in Table 2, several observations are obtained as follows:

- (1) NRG01 granite samples have a higher peak strength than TMS01 samples under various confinements ranging from 0–30 MPa. The existence of biotite and gneissosity may be two main reasons reducing the strength of TMS01 granite samples.
- (2) In general, NRG01 granite samples have comparable peak strength values as BS06 granite samples under different confinements. In a more detailed comparison, it can be found that NRG01 samples have lower peak strength under low confinements, while higher peak strength under high confinements than BS06 samples. This observation is consistent with the results presented in Table 1, i.e., NRG01 samples have lower  $\sigma_{ci}$  and  $c$  values while higher  $m_i$  and  $\phi$  values than BS06 samples. This may be caused by the different grain sizes. Compared with Figures 11b and 13, it is apparent that NRG01 samples have much larger grain scales than TMS01 samples. Eberhardt et al. [25] found that rock strength will decrease with increasing grain size under uniaxial compression, as larger grains may supply longer paths of weakness for growing cracks to propagate along. This finding can explain the lower peak strength of NRG01 samples with a larger grain size under low confinements well. With the increasing confinement, shear failure becomes the dominant failure mode, and larger grain sizes make it difficult to form shear planes; therefore, the inner frictional angle increases. The recommended values  $m_i$  proposed by Hoek show that the coarse texture may result in a higher  $m_i$  value for the same rock group [26], which is also consistent with the test results in this study.

Laboratory studies on the strength properties of the cored samples show that TMS01 granite has significantly lower strength than NRG01 granite under different confinements. Therefore, more detailed research should focus on NRG01 granite samples.

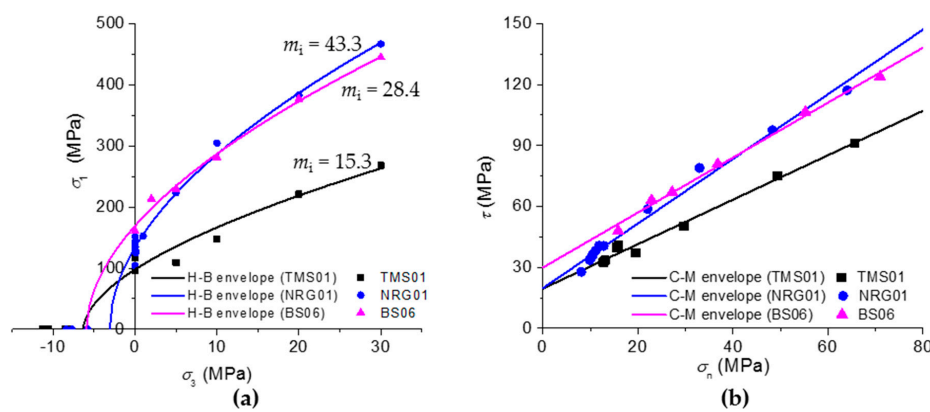


**Figure 12.** (a) Hoek–Brown envelopes and (b) Coulomb–Mohr envelopes based on the uniaxial and triaxial test results on the TMS01 and NRG01 samples, compared with the results on the BS06 samples from the Beishan area, Gansu Province [21].

**Table 2.** Strength properties of the cored granite samples.

Samples	$m_i$	$\sigma_{ci}$ (MPa)	$c$ (MPa)	$\phi$ (°)
TMS01 granite	15.3	97.9	19.9	47.2
NRG01 granite	43.3	134.4	20.1	57.5
BS06 granite [21]	28.4	169.3	30.2	53.3

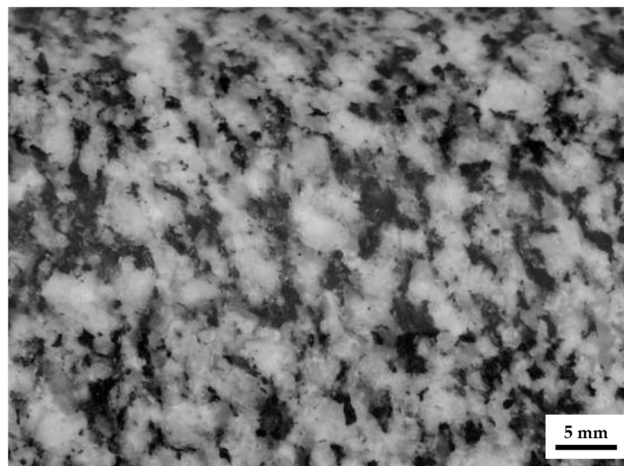


Figure 13. Grain scales and distribution of BS06 samples from the Beishan area, Gansu Province [27].

#### 4. Dynamic Effect on the Mechanical Properties of NRG01 Granite

Disturbance during the construction induced by excavation and seismicity during the operation induced by earthquakes may both have influences on the stability of underground space. It should be noted that different magnitudes of the disturbances from different distances will lead to dynamic loading with different strain rates on the surrounding rock mass [28]. Therefore, it is necessary to study the effect of strain rate on the strength properties and failure patterns of the host rock.

Uniaxial compressive tests under various strain rates ( $1.0 \times 10^{-5}$ ,  $1.0 \times 10^{-4}$ ,  $1.0 \times 10^{-3}$  and  $0.6 \times 10^{-2} \cdot s^{-1}$ ) have been conducted on NRG01 granite samples. It is noted here that the highest strain rate in this study was set to be  $1.0 \times 10^{-2} \cdot s^{-1}$  when the tests were conducted; however, the true strain rate of the sample is  $0.6 \times 10^{-2} \cdot s^{-1}$  actually, because the test machine cannot be absolutely stiff, and the deformation of the machine cannot be ignored at such a high strain rate.

Peak strength and failure patterns obtained from the tests are presented in Figures 14 and 15, respectively. Generally speaking, a higher strain rate leads to a higher peak strength, but UCS increases only about 19.3% from the rate of  $1.0 \times 10^{-5}$ – $0.6 \times 10^{-2} \cdot s^{-1}$ . However, the failure patterns show a more significant influence of strain rate. Under the strain rate of  $1.0 \times 10^{-5} \cdot s^{-1}$ , only a few tensile fractures can be observed in the sample. When the strain rate increases to  $1.0 \times 10^{-4} \cdot s^{-1}$ , more fractures occur, and many tiny particles fly out from the fractures; however, the sample can still stand there and keeps the general cylindrical shape. Under the strain rates of  $1.0 \times 10^{-3}$  and  $0.6 \times 10^{-2} \cdot s^{-1}$ , violent failure happens with a loud noise, and the sample is totally fractured with many fragments with different sizes thrown at different distances. These test results show that increasing strain rate may increase the UCS of NRG01 granite samples to a little higher value; however, it will also result in a much more violent failure of the samples owing to a sudden release of energy.

Compared with the conventional uniaxial compressive test under the strain rate of  $0.6 \times 10^{-2} \cdot s^{-1}$ , another test is conducted on an NRG01 granite sample packed with a heat shrinkable tube under the same strain rate. The heat shrinkable tube is usually used in the triaxial compressive test to isolate the sample from the oil in the loading cell. Interestingly, it is found that the peak strength of the sample increases only by 7.3% packed with the heat shrinkable tube; however, the failure is much more stable (Figure 16). Although the sample is also quite fractured, no fragments have been thrown, and the sample almost retains its original shape. The soft ductile tube dissipates much of the energy released suddenly; consequently, the failure occurs in a stable manner under such a high strain rate. This test result shows that a soft ductile support cannot increase the strength of the surrounding rock mass significantly; nevertheless, it is very useful to protect the underground opening from a violent failure.

The conventional triaxial compressive tests are also conducted on NRG01 samples under different strain rates. Figure 17 shows the peak strengths of the samples from the tests under strain rates of

$1.0 \times 10^{-5}$  and  $0.6 \times 10^{-2} \cdot s^{-1}$  and the confinements ranging from 0–10 MPa. It is observed that both Hoek–Brown and Coulomb–Mohr peak strength envelopes are almost parallel with their cases under different strain rates, which shows that with increasing strain rate, the Hoek–Brown parameter  $m_i$  and inner frictional angle  $\phi$  almost keep constant, while cohesion  $c$  increases. This observation is consistent with the conclusion in [28]. Compared with the results from the uniaxial compressive tests, the strain rate has a less obvious influence on the failure patterns under the confinements. Higher strain rates always result in more fractures; however, the confinement, even if as low as 1 MPa, keeps the sample from violent failure.

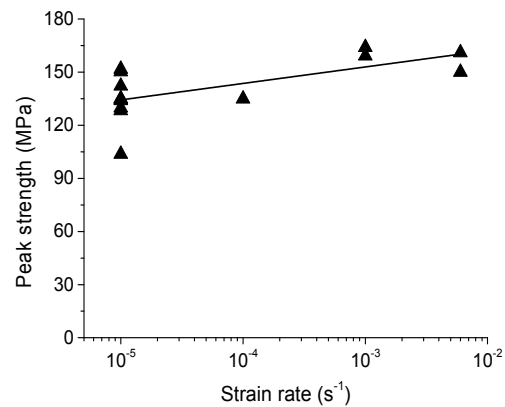


**Figure 14.** Peak strength of NRG01 granite samples under various strain rates in uniaxial compressive tests.



**Figure 15.** Failure modes of NRG01 granite samples under the strain rates of (a)  $1.0 \times 10^{-5} \cdot s^{-1}$ ; (b)  $1.0 \times 10^{-4} \cdot s^{-1}$ ; (c)  $1.0 \times 10^{-3} \cdot s^{-1}$  and (d)  $0.6 \times 10^{-2} \cdot s^{-1}$  in uniaxial compressive tests.



**Figure 16.** Failure modes of an NRG01 granite sample packed with a heat shrinkable tube under the strain rate of  $0.6 \times 10^{-2} \cdot s^{-1}$  in uniaxial compressive tests.

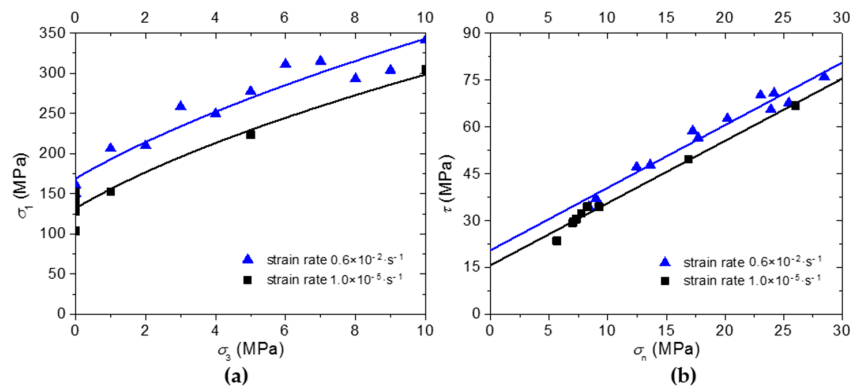


**Figure 17.** (a) Hoek–Brown envelopes and (b) Coulomb–Mohr envelopes of NRG01 granite samples under various strain rates.

### 5. Thermal Effect on the Mechanical Properties of NRG01 Granite

The high-level radioactive waste will produce heat and may have a thermal effect on the surrounding rock mass in the underground storage [29]; hence, the effect of temperature on the strength of host rock plays an important role in the assessment of site selection for underground geological disposal. A very wide range of temperatures from room temperature to 600 °C, 800 °C or even higher than 1000 °C has been considered in the previous studies, and the test results always show that the strength of granite decreases with the increasing temperature [30–32]. However, according to the multi-barrier principle used by the international nuclear community for the conceptual designs of HLW disposal, besides the host rock as the natural barrier, the engineered barriers include the waste itself, the canisters and the buffer, which is always low-permeable clay, for embedding the canisters, as well as seals and fills in the holes or tunnels [3]. In fact, the maximum temperature on the surface of waste canisters is usually controlled to be lower than 100 °C–120 °C based on the conceptual designs of different countries [33–36]; therefore, the temperature of the host rock will be even lower. Take the Canadian concept for example; it is expected to lead to an increase of the temperature in the host rock up to 85 °C [2]. Extensive numerical analyses have been carried out to predict the changing temperature. Guo's model shows that the peak temperatures of the canister surface and tunnel surface are 117.0 °C and 69.0 °C, respectively, for a deep repository in Canada [34]. Based on a Japanese concept, five teams from different countries built thermo-hydro-mechanical coupling models, and the predictions show that the maximum temperature of about 75 °C~80 °C will be reached at the surface of the waste canister [37]. According to the geomechanical properties of the Beishan area in China, Liu et al. [38] used a thermo-mechanical model, and the result shows that the maximum temperature of the host rock will reach 80 °C with a 4-m spacing between the tunnels. Consequently, more detailed research should focus on the range closer to the caused temperatures according to the conceptual designs. In this study, various temperatures ranging from 20 °C (room temperature) to 200 °C are considered to research their effects on the strength properties of NRG01 granite samples.

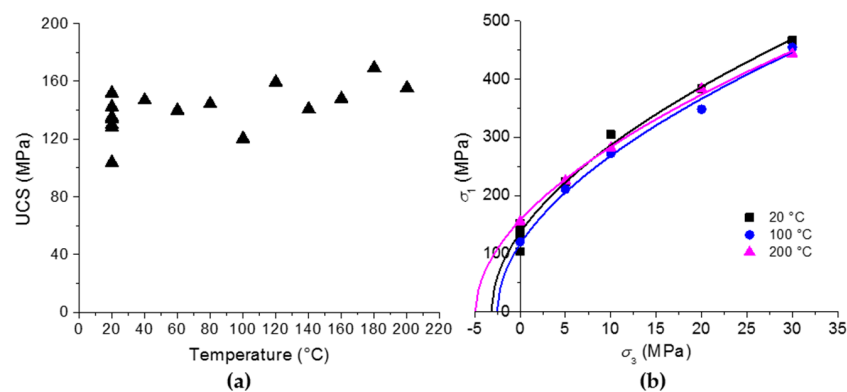
Each sample is heated to the target temperature with a heating rate of about 2 °C/min at first. The heat-treated samples are applied to conduct uniaxial and triaxial compressive tests with an axial strain rate of  $1.0 \times 10^{-5} \cdot \text{s}^{-1}$ .

The uniaxial compressive strengths of NRG01 granite samples affected by different temperatures are plotted in Figure 18a. Generally speaking, the influence of temperature (20 °C–200 °C) on the UCS of NRG01 granite is quite limited. Nevertheless, for a more detailed analysis, it is observed that UCS increased slightly with the increasing temperatures. Similar observations have been reported in [39,40]. In [40], based on the SEM technique, micro-cracks have been observed in Indian granite under various temperatures ranging from 30 °C–160 °C. It should be noted that the width of pre-existing micro-cracks increases from 30 °C–65 °C, corresponding to a slight decrease of UCS; thereafter, the width decreases with increasing temperature, and no obvious development of new micro-cracks has been observed

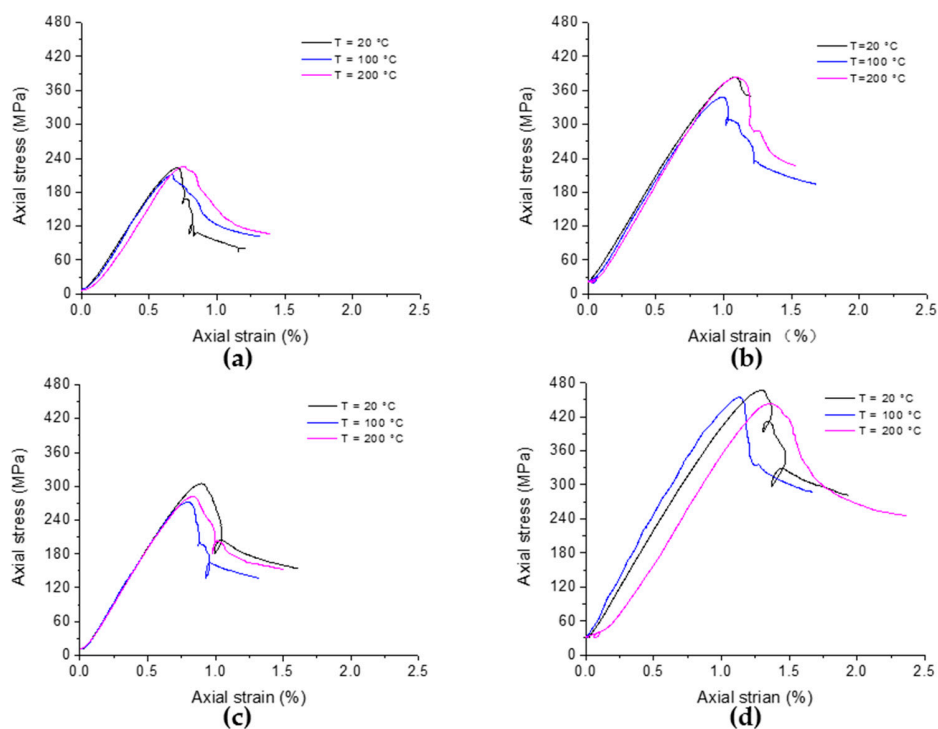
at any temperature up to 160 °C. This finding may be helpful to analyze the strength characteristics under various temperatures; however, more detailed observations on the effect of temperature on the behaviors of micro-cracks and minerals of NRG01 granite should be conducted in future work.

Figure 18b presents the peak strength of heat-treated NRG01 granite samples (20 °C, 100 °C and 200 °C) under various confinements (0, 5, 10, 20 and 30 MPa), and it is found that the Hoek–Brown envelopes are very close. On the whole, temperature (20 °C–200 °C) has quite limited influence on the peak strength of NRG01 granite samples under various confinements (0–30 MPa).

The complete stress-strain curves of the tests on NRG01 granite samples under different temperatures (20 °C, 100 °C and 200 °C) and confinements (5, 10, 20 and 30 MPa) are plotted in Figure 19. Under each confinement, the temperature has no obvious influence on the pre-peak behavior of NRG01 samples; however, it is observed that a higher temperature may lead to a more ductile post-peak behavior.



**Figure 18.** Thermal effect on the (a) uniaxial compressive strength and (b) failure envelope of NRG01 granite samples.



**Figure 19.** Thermal effect on axial stress-strain curves of NRG01 granite samples under the confinement of: (a) 5 MPa; (b) 10 MPa; (c) 20 MPa; and (d) 30 MPa.

## 6. Conclusions

Geomechanical study is very important in site selection for safe geological disposal of HLW. Rock mass quality and strength properties of the rock material should be considered to evaluate the stability of the host rock. In addition, disturbance induced by the underground excavation and earthquakes, as well as the heat produced by HLW should also be studied for their effects on rock stability.

Surface investigations show that the NRG sub-area has massive granite intrusions, while the outcrops in the TMS sub-area are seriously weathered and jointed. RQD analyses on the core logs from four 600-m sub-vertical boreholes also show that the deep rock mass quality in the NRG sub-area is better, and NRG01 cored samples present the best quality, which is comparable with the good cases in the Beishan area, Gansu province.

Laboratory uniaxial and triaxial compressive tests on the well-prepared samples from the drill cores show that NRG01 granite samples have higher peak strength under various confinements ranging from 0–30 MPa than TMS01 samples, and it is found that the lower strength of TMS01 samples is caused by the existence of biotite and gneissosity. NRG01 samples have generally comparable peak strength under various confinements as BS06 samples from the Beishan sub-area; however, the larger grain scales lead to lower  $\sigma_{ci}$  and  $c$  values, while higher  $m_i$  and  $\phi$  values for the NRG01 samples.

Uniaxial and triaxial compressive tests under different axial strain rates supply a way to study the effect of disturbance with different magnitudes on the stability of rock. Increasing the strain rate from  $1.0 \times 10^{-5}$ – $0.6 \times 10^{-2}$ ·s<sup>-1</sup> can only increase the UCS of NRG01 granite samples by about 19.3%; however, it can result in much more violent failure. It is found that the heat shrinkable tube can dissipate considerable energy released suddenly and protect the sample from a violent failure, which means that the soft ductile support has a limited effect on strengthening the host rock, but it is very useful in preventing the underground opening from a violent failure. It is also found that the peak strength of NRG01 samples under various confinements (0–10 MPa) increases with the increasing strain rate; however, Hoek–Brown parameter  $m_i$  and inner frictional angle  $\phi$  almost keep constant, but cohesion  $c$  increases significantly.

Temperatures ranging from 20 °C–200 °C have a limited effect on the peak strength of NRG01 granite samples under various confinements (0–30 MPa). However, from a more detailed perspective, the UCS of NRG01 granite increases slightly with the increasing temperatures. Complete stress-strain curves obtained from triaxial compressive tests show that the pre-peak behavior of NRG01 samples is almost independent of the changing temperature, while the post-peak behavior becomes more ductile with the temperature changing from 20 °C–200 °C.

Based on the field and laboratory studies on the site selection for HLW disposal in the Alxa area, the NRG sub-area has massive granite intrusions, and NRG01 cored granite samples have higher strength than TMS01 samples. The geomechanical properties of NRG01 granite considering various strain rates and temperatures can also supply parameters for the modelling analysis in further studies. However, this paper only covers some basic geomechanical studies for a series of comparing analyses on different candidate areas, and more extensive and rigorous in situ and laboratory research must be carried out to give reliable data for the safety design of the repository. For example, more boreholes should be drilled in the NRG sub-area to make clear the structure and mechanical properties of the rock mass. In addition, the seepage properties of the cored samples should also be studied to evaluate the risk of radionuclide migration. Due to the long-lasting period of geological storage, the creeping behavior of the host rock is also very important. Furthermore, for an expected area for HLW disposal, underground laboratory geomechanical tests should be conducted considering the in situ complex conditions including the in situ stresses, rock mass structures, water conditions, etc., and the influence of excavation methods and temperature on the damage of the surrounding rock mass should also be taken into consideration. These studies will be conducted in future work.

**Acknowledgments:** This work is financially supported by National Natural Science Foundation of China (No. 41402286), the High-Level Radioactive Waste Disposal Project of the State Administration for Science, Technology and Industry for National Defense, China, the Strategic Priority Research Program of the Chinese

Academy of Sciences (Grant No. XDB10030301), and National Science and Technology Major Project (No. 2016ZX05034003-005). Yu Wang, Zheng Yang, Yusong Wu, Yanhui Dong, and Fan Song are appreciated for their help in this study. The anonymous reviewers gave very helpful suggestions, which were valuable for improving our manuscript.

**Author Contributions:** Cheng Cheng conducted the field investigation and laboratory experiments, as well as the analyses. Xiao Li and Shouding Li conceived of and designed the experiments and guided the study. Bo Zheng played an important role in performing the experiments. Cheng Cheng wrote the paper.

**Conflicts of Interest:** The authors declare no conflict of interest.

## Abbreviations

The following abbreviations are used in this manuscript:

HLW	High-level radioactive waste
UCS	Uniaxial compressive strength
RQD	Rock quality designation index
TMS	Tamusu
NRG	Nuorigong
BS	Beishan
ISRM	International Society for Rock Mechanics
H-B	Hoek–Brown
C-M	Coulomb–Mohr
GSI	Geological strength index
GPS	Global Positioning System
SEM	Scanning electron microscope

## References

1. Martino, J.B.; Chandler, N.A. Excavation-induced damage studies at the underground research laboratory. *Int. J. Rock Mech. Min. Sci.* **2004**, *41*, 1413–1426. [[CrossRef](#)]
2. Read, R.S. 20 years of excavation response studies at AECL's underground research laboratory. *Int. J. Rock Mech. Min. Sci.* **2004**, *41*, 1251–1275. [[CrossRef](#)]
3. Pusch, R. *Geological Storage of Highly Radioactive Waste*; Springer: Berlin, Germany, 2009.
4. Zhao, X.G.; Wang, J.; Cai, M.; Ma, L.K.; Zong, Z.H.; Wang, X.Y.; Su, R.; Chen, W.M.; Zhao, H.G.; Chen, Q.C.; et al. In-situ stress measurements and regional stress field assessment of the Beishan area, China. *Eng. Geol.* **2013**, *163*, 26–40. [[CrossRef](#)]
5. Zhao, X.G.; Wang, J.; Qin, X.H.; Cai, M.; Su, R.; He, J.G.; Zong, Z.H.; Ma, L.K.; Ji, R.L.; Zhang, M.; et al. In-situ stress measurements and regional stress field assessment in the Xinjiang candidate area for China's HLW disposal. *Eng. Geol.* **2015**, *197*, 42–56. [[CrossRef](#)]
6. Kim, J.-S.; Kwon, S.-K.; Sanchez, M.; Cho, G.-C. Geological storage of high level nuclear waste. *KSCE J. Civ. Eng.* **2011**, *15*, 721–737. [[CrossRef](#)]
7. Hudson, J.A. Underground radio active waste disposal: The rock mechanics contribution. In Proceedings of the ISRM International Symposium—6th Asian Rock Mechanics Symposium, New Delhi, India, 23–27 October 2010.
8. Fairhurst, C. Nuclear waste disposal and rock mechanics: Contributions of the underground research laboratory (URL), pinawa, manitoba, canada. *Int. J. Rock Mech. Min. Sci.* **2004**, *41*, 1221–1227. [[CrossRef](#)]
9. Martin, C.D. Preliminary Assessment of Potential Underground Stability (Wedge and Spalling) at Forsmark, Simpevarp and Laxemar sites. Available online: <http://www.skb.se/upload/publications/pdf/R-05-71.pdf> (accessed on 14 July 2016).
10. Wang, J. High-level radioactive waste disposal in China: Update 2010. *J. Rock Mech. Geotech. Eng.* **2010**, *2*, 1–11.
11. Wang, J. On area-specific underground research laboratory for geological disposal of high-level radioactive waste in China. *J. Rock Mech. Geotech. Eng.* **2014**, *6*, 99–104. [[CrossRef](#)]
12. Zhao, X.G.; Wang, J.; Cai, M.; Cheng, C.; Ma, L.K.; Su, R.; Zhao, F.; Li, D.J. Influence of unloading rate on the strainburst characteristics of Beishan granite under true-triaxial unloading conditions. *Rock Mech. Rock Eng.* **2014**, *47*, 467–483. [[CrossRef](#)]
13. Song, F.; Dong, Y.-H.; Xu, Z.-F.; Zhou, P.-P.; Wang, L.-H.; Tong, S.-Q.; Duan, R.-Q. Granite microcracks: Structure and connectivity at different depths. *J. Asian Earth Sci.* **2016**, *124*, 156–168. [[CrossRef](#)]

14. Shi, X.; Wang, T.; Zhang, L.; Castro, A.; Xiao, X.; Tong, Y.; Zhang, J.; Guo, L.; Yang, Q. Timing, petrogenesis and tectonic setting of the Late Paleozoic gabbro–granodiorite–granite intrusions in the Shalazhashan of northern Alxa: Constraints on the southernmost boundary of the Central Asian Orogenic Belt. *Lithos* **2014**, *208*, 158–177. [[CrossRef](#)]
15. Shi, X. The Tectonic Affinity of the Zongnaishan-Shalazhashan Zone in Northern Alxa and Its Implications: Evidence from Intrusive and Metamorphic Rocks. Ph.D. Thesis, Chinese Academy of Geological Sciences, Beijing, China, 2015. (In Chinese)
16. Niu, Z.; Wang, M.; Sun, H.; Sun, J.; You, X.; Gan, W.; Xue, G.; Hao, J.; Xin, S.; Wang, Y.; et al. Contemporary velocity field of crustal movement of Chinese mainland from global positioning system measurements. *Chin. Sci. Bull.* **2005**, *50*, 939–941. [[CrossRef](#)]
17. Xue, R.H.; An, Z.G.; Wang, X.X.; Di, Q.Y. Probing inner structure of rock mass at a high-level radioactive preselected site in Tamusu, Inner Mongolia. *Chin. J. Geophys.* **2016**, *59*, 2316–2325. (In Chinese)
18. Deere, D.U. Geological considerations. In *Rock Mechanics in Engineering Practice*; Stagg, K.G., Zienkiewicz, O.C., Eds.; John Wiley and Sons: New York, NY, USA, 1968; pp. 1–20.
19. Fairhurst, C.E.; Hudson, J.A. Draft ISRM suggested method for the complete stress-strain curve for the intact rock in uniaxial compression. *Int. J. Rock Mech. Min. Sci.* **1999**, *36*, 279–289.
20. Bieniawski, Z.T.; Bernede, M.J. Suggested methods for determining the uniaxial compressive strength and deformability of rock materials. *Int. J. Rock Mech. Min. Sci. Geomech. Abstr.* **1979**, *16*, 138–140. [[CrossRef](#)]
21. Chen, L.; Liu, J.; Wang, C.; Wang, X.; Su, R.; Wang, J.; Shao, J. Elastoplastic damage model of Beishan deep granite. *Chin. J. Rock Mech. Eng.* **2013**, *32*, 289–298. (In Chinese)
22. Hoek, E.; Carranza-Torres, C.; Corkum, B. Hoek-brown failure criterion-2002 edition. In Proceedings of the 5th North American Rock Mechanics Symposium and the 17th Tunnelling Association of Canada Conference: NARMS-TAC 2002, Toronto, ON, Canada, 7–10 July 2002.
23. Hoek, E.; Wood, D.; Shah, S. A modified Hoek-Brown criterion for jointed rock masses. In Proceedings of the Rock Characterization: ISRM Symposium, Eurock'92, Chester, UK, 14–17 September 1992; Hudson, J.A., Ed.; pp. 209–214.
24. Brady, B.H.; Brown, E.T. *Rock Mechanics: For Underground Mining*, 3rd ed.; Springer: Dordrecht, The Netherlands, 2006; pp. 105–107.
25. Eberhardt, E.; Stimpson, B.; Stead, D. Effects of grain size on the initiation and propagation thresholds of stress-induced brittle fractures. *Rock Mech. Rock Eng.* **1999**, *32*, 81–99. [[CrossRef](#)]
26. Hoek, E. *Practical Rock Engineering (2007 Edition)*; Rocscience: Toronto, ON, Canada, 2007. Available online: <http://www.rocscience.com> (accessed on 14 July 2016).
27. Zhao, X.; Like, M.A.; Rui, S.U.; Ju, W. Fracture evolution and strength characteristics of Beishan deep granite under compression conditions. *Chin. J. Rock Mech. Eng.* **2014**, *33*, 3665–3675. (In Chinese)
28. Zhao, J. Applicability of Mohr–Coulomb and Hoek–Brown strength criteria to the dynamic strength of brittle rock. *Int. J. Rock Mech. Min. Sci.* **2000**, *37*, 1115–1121. [[CrossRef](#)]
29. Wanne, T.S.; Young, R.P. Bonded-particle modeling of thermally fractured granite. *Int. J. Rock Mech. Min. Sci.* **2008**, *45*, 787–799. [[CrossRef](#)]
30. Chen, Y.-L.; Ni, J.; Shao, W.; Azzam, R. Experimental study on the influence of temperature on the mechanical properties of granite under uni-axial compression and fatigue loading. *Int. J. Rock Mech. Min. Sci.* **2012**, *56*, 62–66. [[CrossRef](#)]
31. Xu, X.; Kang, Z.; Ji, M.; Ge, W.; Chen, J. Research of microcosmic mechanism of brittle-plastic transition for granite under high temperature. *Procedia Earth Planet. Sci.* **2009**, *1*, 432–437.
32. Takarli, M.; Prince-Agbodjan, W. Temperature effects on physical properties and mechanical behavior of granite: Experimental investigation of material damage. *J. ASTM Int.* **2008**, *5*, 100464–100476.
33. Weetjens, E. Update of the Near Field Temperature Evolution Calculations for Disposal of UNE-55, MOX-50 and Vitrified HLW in a Supercontainer-Based Geological Repository. Available online: [http://publications.sckcen.be/dspace/bitstream/10038/1039/1/er\\_86.pdf](http://publications.sckcen.be/dspace/bitstream/10038/1039/1/er_86.pdf) (accessed on 13 July 2016).
34. Guo, R. Coupled Thermal-Mechanical Modelling of a Deep Geological Repository Using the Horizontal Tunnel Placement Method in Sedimentary Rock Using CODE\_BRIGHT. Available online: [https://www.nwmo.ca/~media/Site/Reports/2015/09/24/05/33/1695\\_nwmotr-2010-22horizontal-tunnel-placmentmethod\\_limestone\\_r0b\\_worddocument.ashx?la=en](https://www.nwmo.ca/~media/Site/Reports/2015/09/24/05/33/1695_nwmotr-2010-22horizontal-tunnel-placmentmethod_limestone_r0b_worddocument.ashx?la=en) (accessed on 13 July 2016).

35. Ikonen, K. Thermal Analyses of Spent Nuclear Fuel Repository. Available online: [http://www.posiva.fi/files/1018/Posiva\\_2003-04.pdf](http://www.posiva.fi/files/1018/Posiva_2003-04.pdf) (accessed on 13 July 2016).
36. International Atomic Energy Agency (IAEA). Geological Disposal of Radioactive Waste: Technological Implications for Retrievability. Available online: [http://www-pub.iaea.org/MTCD/publications/PDF/Pub1378\\_web.pdf](http://www-pub.iaea.org/MTCD/publications/PDF/Pub1378_web.pdf) (accessed on 14 July 2016).
37. Rutqvist, J.; Chijimatsu, M.; Jing, L.; Millard, A.; Nguyen, T.S.; Rejeb, A.; Sugita, Y.; Tsang, C.F. A numerical study of THM effects on the near-field safety of a hypothetical nuclear waste repository—BMT1 of the DECOVALEX III project. Part 3: Effects of THM coupling in sparsely fractured rocks. *Int. J. Rock Mech. Min. Sci.* **2005**, *42*, 745–755. [[CrossRef](#)]
38. Liu, W.; Wang, J.; Zhou, H.; Yang, C.; Jiang, P. Coupled thermo-mechanical analysis of granite for high-level radioactive waste repository. *Chin. J. Rock Mech. Eng.* **2009**, *28*, 2875–2883. (In Chinese)
39. Huang, Y.; Xia, X. Physical effect on fracture toughness of rock. *Chin. J. Geotech. Eng.* **1987**, *9*, 91–96. (In Chinese)
40. Dwivedi, R.D.; Goel, R.K.; Prasad, V.V.R.; Sinha, A. Thermo-mechanical properties of Indian and other granites. *Int. J. Rock Mech. Min. Sci.* **2008**, *45*, 303–315. [[CrossRef](#)]



© 2016 by the authors; licensee MDPI, Basel, Switzerland. This article is an open access article distributed under the terms and conditions of the Creative Commons Attribution (CC-BY) license (<http://creativecommons.org/licenses/by/4.0/>).